ORIGINAL PAPER

PCB-waste derived resin as a binary ion exchanger for zinc removal: Isotherm modelling and adsorbent optimization

Shifa Zuhara[1] · Gordon McKay[1]

Abstract

Effective removal of heavy metals from wastewaters can enable increased reuse of treated wastewater and reduce water scarcity worldwide. This paper describes the results of an initial study on zinc removal using waste-derived aluminosilicate-based material by binary ion exchange with calcium and potassium. About 2 mmol/g of zinc removal adsorption capacity was demonstrated using the aluminosilicate resin. Seven equilibrium isotherm models have been analyzed using the zinc adsorption data; the best fit to the experimental values based on the lowest SSE error was the SIPS model. A mechanism between zinc adsorption and the calcium and potassium desorption has been developed and modelled and is confirmed based on the mass balance analysis between the divalent calcium ions and the monovalent potassium ions exchanged with the divalent zinc ions adsorbed. Desorption studies using isotherm model equations for the calcium and potassium data further confirmed the mechanism. Regeneration was over 80% per cycle for three acid regenerations, indicating the zinc can be recovered for re-use. Furthermore, optimization using the SIPS model showed the minimum amount of adsorbent required using a two-stage reactor system is much lower, proving the need for a two-stage reactor to make the system more economical. Future experiments on multicomponent analysis and further optimization will help develop this adsorbent for real water systems.

Abbreviations

NMF	Non-metallic fraction
A-NMF	Activated non-metallic fraction
CHNS	Carbon, hydrogen, nitrogen, and sulfur
XRF	X-ray fluorescence
FTIR	Fourier transform spectroscopy
BET	Brunauer–Emmett–Teller
XPS	X-ray Photoelectron spectrometry
SEM–EDX	Scanning electron microscopy with energy dispersive X-ray spectroscopy
SA	Surface area
PV	Pore volume
SSE	Sum of error squares

✉ Shifa Zuhara
szuhara@hbku.edu.qa

1   Division of Sustainable Development, College of Science and Engineering, Hamad Bin Khalifa University, Education City, Qatar Foundation, Doha, Qatar

Introduction

Water scarcity is a significant global problem, and according to the World Economic Forum, it is among the top five global risks from 2012 to 2019. Rising population, developing economy, and changing global climate have recently led to water scarcity (Zhang et al. 2021). Increasing water needs for water in terms of aquifer recharge, irrigation and drinking are making use of growing volume of treated wastewater (Mendret et al. 2019). Similarly, the increase in population is proportional to the number of wastes produced globally; the million tons of organic and inorganic waste, both municipal and industrial waste being dumped yearly are responsible for harmful environmental emissions (Nowicki et al. 2016). Therefore, it is beneficial to convert these wastes to value-added products and this is considered a better alternative to other solid waste management techniques such as combustion and incineration as it enables a circular economy while protecting the environment (Mariyam et al. 2022a).

Water pollution associated industrial activities have been an issue persistent for a long time now. Among the pollutants present in wastewater, heavy metals from industrial sources are of concern due to their persistent and non-degradable

nature. In particular, zinc which is one of the major heavy metals known to problematic due to its toxic nature, with several industrial sources such as mining, galvanization, stabilizers, steel production, coal burning, and zinc purification (Chakraborty et al. 2022). The associated bioaccumulation and biomagnification are known to cause trouble in the environment. Additionally, a high concentration of heavy metals is known to be toxic and to disrupt the metabolism of a cell, which in turn effects the cerebral and nervous function and organs such as lungs, kidney and others (Carolin et al. 2017). Therefore, stringent limits for heavy metals have been set by authorities such as the US-EPA to ensure proper disposal of the effluents from industries- for example, for zinc the maximum permissible limit is 1 mg/L (Bilal et al. 2022).

It is important to adopt a technology for removing these heavy metals from wastewater effectively to such minimal levels. According to Shrestha et al. (2021), technologies including photocatalysis, electrodialysis, membrane separation technique, and adsorbents are promising for removing heavy metals. Compared to the other methods, the adsorption method is most promising owing to its relatively lower operation costs and high removal efficiencies; moreover, adsorption gives the best option regarding technical feasibility at the industrial level (Mangwandi et al. 2016). However, adsorption has two main disadvantages: availability and cost-effectiveness (Carolin et al. 2017). But there are widely available low-cost wastes for water treatment combat such problems (Joseph et al. 2019).

Several studies showed the successful removal of zinc from water. In recent literature, several waste feeds is reported with good zinc removal rates such as corn cob (Lestari et al. 2020), tea waste (Çelebi et al. 2020), waste tire (Cherono et al. 2021) and more interestingly, research compares different kinds of waste feedstocks. One such study compared three different agricultural wastes namely rice husk, coconut coir and moringa seeds all showing excellent adsorption capacities (> 16.1 mg/g). Quite similarly, another study investigated bamboo, wood, and rice husk biochar samples revealing best adsorption capacity by bamboo biochar (7.62 mg/g) (Van Hien et al. 2020). Another study focused on using different kinds of fruit peels from orange, pineapple and pomegrate sources, all showed zinc adsorption capacities greater than 36 mg/g (Turkmen Koc et al. 2021). Although there are several works detailing the use of biomass related waste (evident from the discussion above), utilizing electronic wastes (e-wastes) for the same have not been explored to date. With the technological advancement observed around the world, in addition to the short life span of electronic goods, there is an exponential rise in the waste being produced with a predicted rise to 74 million tons by 2030 which is significantly higher than the 53.6 million tons generated in 2019 (Wu et al. 2022). As part of the electronic equipment, around 3–7% is the printed circuit boards

(PCBs) which forms a significant, useable portion after separation of the e-waste (Wu et al. 2022). Usually, separation is carried out as part of the recycling process of this waste into the metallic and non-metallic fractions; the expensive, recoverable metals are recovered, and the non-metal fractions are incinerated. This study utilizes the non-metallic fraction for water treatment, specifically for the removal of zinc from water. There is only limited application of adsorbents or resins made from this waste in such a manner. One study focused on removing methylene blue from water using activated non-metallic fraction (NMF)- 98% from a 10 mg/mL of adsorbate was revealed (Muthuraman et al. 2020). Another study focused on removing the pharmaceuticals diclofenac and ibuprofen by producing Fenton-like catalysts from PCBs showing good removal rates from water (Rahman and Aziz 2022). Two studies on heavy metal removal have also been reported recently (Xu et al. 2021; Mariyam et al. 2022b). However, this study uniquely investigates the removal of zinc from water in both single and two-stage adsorption systems by minimizing the total mass adsorbent.

- The main objectives of this paper are to (1) measure the adsorption capacity using the novel e-waste-derived adsorbent, (2) propose a new binary model using the adsorbent for ion exchange with calcium and potassium ions, (3) conduct isotherm modelling for zinc removal (single system) to understand the capacity of the system (4) optimize a two-stage batch adsorption system to minimize the adsorbent mass required- this is essential to remove the pollutant to the desired treated effluent concentration limit value while reducing the amount of adsorbent used, making the system more economical in terms of operational costs. understand the capacity of the system further

Methodology

Materials

Chemical and materials used

The raw material used in this study was obtained from an e-waste processing plant in Hong Kong that disintegrates the printed circuit board wafers (Ning et al. 2017b). The waste printed circuit boards are shredded and disintegrated by high velocity impact into a powder of an average size around a few hundred microns. This powder product comprises a metallic copper fraction and a non-metallic aluminosilicate based fraction. This powder product is then pneumatically passed through a high efficiency corona electrostatic separator which separates the two fractions. The copper containing metallic fraction is sold and undergoes refining by smelting

to recover pure copper. However, the non-metallic fraction (NMF) has no apparent use and was used as the raw material in this research to produce a high quality aluminosilicate ion exchange resin having a mean diameter around two to three hundred micrometers. The appearance of this NMF fraction is a fine greenish-grey powder with no odour, and possessing characteristic properties such as a low porosity and a high hydrophobicity and in this form it has no ion exchange potential. This raw material was collected from the e-waste processing plant and brought back to the university for further development, treatment and testing. The other chemical materials used in the study include:—potassium hydroxide and zinc nitrate, which were obtained from Sigma-Aldrich Company. Deionized water was used in this study to produce the metal ion solutions and was prepared using a Milli-Q Integral Water purification system.

Activation process to aluminosilicate resin

The NMF of printed circuit board e-waste was added to potassium hydroxide, KOH (1:2), and continuously mixed at ambient temperature for 3 h. The weight ratio of KOH to NMF (ratio of impregnation) was kept stable at 2; this was further heated for 3 h to 250 °C using a heating rate of 5 °C/min in a Carbolite muffle furnace of a volume of eighteen liters (AAF11/18, Carbolite, UK) in a nitrogen atmosphere with a purity 99.9%. After the reaction period the produced material was cooled to ambient temperature with an inert nitrogen atmosphere. To remove any unreacted activating material and to neutralize the supernatants pH, the activated material component, A-NMF, was rinsed with hot water for 30 min; finally, the material was dried for 24 h at 110 °C and stored in a desiccator.

Characterization methods

The procedures for characterization of the e-waste derived adsorbent are outlined but the results have been presented and discussed in detail in two previous studies (Ning et al. 2016; Hadi et al. 2015).

Elemental analysis

Elemental CHNS (carbon, hydrogen, nitrogen, and sulfur) analysis of the samples was carried out using an elemental analyser instrument (Elementar Vario EL III, Varian, Germany). About 5 mg of the sample was kept in a foiled container after weighing. Further, the substance is combusted by cracking at 1423 K in a reductive atmosphere. Finally, the electrical conductivity between the combusted gases and helium gas (reference) was measured to study the composition of the samples.

X-ray fluorescence (XRF) technique (JSX-3201Z, Jeol) was used to conduct a qualitative assessment on the elemental composition of the samples. The procedures are presented but the results have been presented in two previous papers.

Fourier transform spectroscopy (FTIR)

FTIR analysis was conducted in order to find the bonding information in the samples. It was conducted using FTIR spectroscopy (Spectrum GX, Perkin Elmer FTIR). It was recorded from 500 to 4000 cm^{-1}. Before analysis, the required samples were mixed with potassium bromide (KBr) at a ratio of 1:100 prior to compressing into a flat disc. To provide a background scan, we prepared a disc of just KBr for analysis.

Nitrogen adsorption–desorption studies/ BET analysis

Surface area (SA) measurement of the samples (NMF and A-NMF) was conducted using adsorption–desorption of nitrogen by an Autosorb1-Quantachrome Brunauer–Emmett–Teller (BET) instrument at 77 K. Before the outgassing process, the samples were kept in a desiccator. The process involves removing the moisture and impurities physically adsorbed on the surface of the solid at 150 degrees for 3 h. Furthermore, the specific area of the surface material and the monolayer adsorption capacity were calculated using the following equation:

$$S_{\mathrm{BET}-N_2} = q_{mN_A A_M} \tag{1}$$

where: $S_{\mathrm{BET-N2}}$ is the BET SA (m^2/g), q_m is the quantity of nitrogen adsorbed in the monolater (mol/g), N_A is Avogadro number (6.023×10^{23} molecules/mol) and A_m is nitrogen's projected area (16.2×10^{-20} m.^{2} at 77 K)

X-ray photoelectron spectrometry (XPS)

XPS was performed to study the elemental composition of the chemicals on the surface of the material including the elemental composition, concentrations and chemical states. In this study, XPS studies were carried out using an XPS-PHI5600 system. During the process, the energy source is a monochromatic Al Kα at 10 kV voltage and 15 mA current. Low and high-resolution spectra were obtained at 70 eV and 20 eV pass energy, respectively. As water adsorption is known to affect the results, all the water present is removed by a drying process with vacuum pumping.

Scanning electron microscopy with energy dispersive X-ray spectroscopy (SEM–EDX)

A scanning electron microscope (Jeol JSM-6700F) was used to understand the morphology of the material's surface. For preparation, the samples were dropped on the carbon

tape after being suspended in ethanol. After this, they were coated with several layers of gold. The emitted rays give information about the elemental and chemical composition of the samples.

Experimental work

Methodology for isotherm experiment

Agitated batch experiments were performed using 0.050 g of the novel A-NMF adsorbent sample added into HDPE plastic bottles containing 0.050 L of 5.0 mmol/L zinc nitrate solution. The initial solution pH was controlled at 5 by adding 0.50 M nitric acid solution to compensate for the strong potassium hydroxide activation stage. The final pH value of each sample was determined to ensure the final pH was less than 7.0 therefore ensuring that no precipitation took place. The sample bottles were placed in an orbital shaker thermostatically controlled at 25 °C and which was rotated at 120 rpm over 48 h ensuring that equilibrium has been achieved. The metal ion concentration in the solutions were determined by inductively coupled plasma atomic emission spectroscopy (ICP-AES, Optima 7300DV, PerkinElmer) initially and at equilibrium for zinc, calcium and potassium. Hence, the quantity of zinc adsorbed on the A-NMF material can be obtained using the mass balance relationship between the solid and liquid phases represented by Eq. (2):

$$q_e = \frac{V}{m}\left(C_o - C_e\right) \tag{2}$$

where Co is the initial concentration in mmol/L, Ce is the final equilibrium concentration in mmol/L, *V* is the solution volume in *L*, *m* is the mass of the functionalized A-NMF adsorbent in g.

The samples' initial and final metal ion concentrations for zinc, calcium and potassium were obtained by using an (ICP-OES). Three aspirations were performed for each sample and only concentration values within $\pm 5\%$ were considered acceptable. Additionally, the final solution pH values were determined. All the adsorption experiments and measurements were performed in triplicate, and the results are presented in the tables and figures, are within as error margin of $\pm 5\%$.

Equilibrium isotherm

The preparation involved making 0.50 L zinc nitrate solutions with initial concentrations of 0.5 mmol/L to 7 mmol/L and a pH level of 4.5–5.5 in a single component system; this was prepared by adding 50 mg of adsorbent and shaken at 120 rpm at 25°C until equilibrium. When the equilibrium was achieved samples were taken and filtered, then the pH values were measured and found to be at pH = 6.0 ± 0.3.

Analyses of the initial and final concentrations of zinc, calcium and potassium were done by ICP atomic emission spectroscopy.

Similar studies on adsorption experiments were conducted for the binary system (potassium and calcium) to estimate the adsorption selectivity of this material.

Regeneration experiments

Regeneration experiments are conducted to reuse the adsorbents continually as it is restored to its initial ionic form. After the batch kinetic experiments, the material A-NMF adsorbed metal ions on the surface (M/A-NMF), a suction filtration process was used to separate the Metal/A-NMF from the liquid and then was dried with vacuum oven and stored in desiccator for regeneration study. In the regeneration process, nitric acid was used to wash out the adsorbed metal ions. Different concentrations and contact times were studied in order to find out the optimized regeneration condition. After the washing process with acid, the material was washed with water followed by filtration. The material was then transferred to a vacuum oven for drying and was used in a subsequent batch contact experiment.

Model theory

Equilibrium models

Usually, isotherm models based on the equilibrium conditions are considered for adsorption studies. This is necessary as adsorption goes through different mechanisms, including the external mass transfer of solute onto the sorbent, intraparticle diffusion and surface pore diffusion, chemisorption and ion exchange with surface sites and complexation reactions; it is impossible to determine the rate-controlling step unless there is significant experimental data for representation.

Therefore, in order to optimize the condition of a sorption system, it is essential to have the most suitable correlation for equilibrium curves. In this study, the adsorption isotherms of metals on the sorbents at specific pH, dosage, and the temperature is considered for the curves. Table 1 shows the isotherm models considered in this study to find the best correlations between the concentrations of the solid-phase and the liquid.

In order to evaluate the best fit model, a non-linear sum of error squares (SSE) was calculated for each of these models. An error function is usually incorporated in the case of the non-linear regression method (Terdputtakun et al. 2017). The parameters of the models can be determined by reducing the errors between the experimental and modeled data.

Table 1 Isotherm Model Equations

Isotherm model	Equation	References
Langmuir	$q_e = \frac{K_L C_e}{1 + a_L C_e}$	(Langmuir 1918)
Freundlich	$q_e = a_F C_e^{b_F}$	(Freundlich 1926)
Redlich–Peterson (RP)	$q_e = \frac{K_R C_e}{1 + a_R C_e^{b_R}}$	(Redlich & Peterson 1959)
SIPS or Langmuir–Freundlich (LF)	$q_e = \frac{K_{LF} C_e^{n_{LF}}}{1 + a_{LF} C_e^{n_{LF}}}$	(Sips 1948)
Toth	$Q_e = \frac{Q_m C_e}{\left[K_T + (C_e^n)\right]^{\frac{1}{n}}}$	(Toth 1971)
Temkin	$q_e = B \ln A_T, + B \ln C_e$	(Temkin 1940)
Dubinin-Radushkevich (DR)	$q_e = \left(\frac{Q_m \exp = \left(RT \ln \left(1 + \frac{1}{C_e} \right) \right)^2}{-2E^2} \right)$	(Dubinin 1960)

Further, the solver function in Microsoft Office Excel program was used to find the values of the constants in each of the isotherm equations by the differences in experimental and calculated values using Eq. (3). The best fit model for the experimental data was selected based on the smallest SSE values achieved using the Excel Solver function. Furthermore, similar calculations and analyses were carried out for the Ca and K desorption systems.

$$\text{SSE} = \sum \left(q_{\exp} - q_{\text{cal}} \right)^2 \qquad (3)$$

q_{cal} is the theoretical sorption capacity calculated from each model and $q_{\exp}$ is the experimental adsorbed amount on the material

Further optimization for minimizing the adsorbent mass required for a two-stage system is calculated based on the best fit model obtained from the single-stage system. The calculations are detailed in Sect. "Optimization for minimizing adsorbent mass" along with the results in Sect. "Optimization for minimizing adsorbent mass".

Results and discussion

Materials characterization

Elemental analysis

Elemental analysis of both the raw and activated materials using the CHNS elemental analyzer determines if the activation has taken place. Table 2 shows how activation affected the material's carbon content; compared to the 20 wt% of carbon present before activation, the carbon content in the activated carbon materials is significantly reduced. Activation at a temperature of 250 °C is considered insufficient for such a significant carbon change, however, the presence of calcium and potassium in the sample (Table 3) could have aided in such a result due to their catalytic nature, which is

Table 2 CHNS elemental composition of NMF and A-NMF

Sample ID	Composition (wt%)				
	C	H	N	S	Others (by difference)
NMF	20	0.2	0.7	0	79.1
A-NMF	1.5	0	0.08	0	97.7

Table 3 Composition of principal elements in NMF and A-NMF revealed by XRF

Elemental composition	NMF (mol%)	A-NMF (mol%)
Al	11.4	10.3
Si	50.6	43.4
Ca	29.7	26.6
Ti	0.60	0.60
Fe	0.20	0.30
Cu	1.80	1.40
Br	4.10	0.00
Ba	0.60	0.50
K	0.00	16.9

a common phenomenon previously observed (Parthasarathy et al. 2023).

XRF was used to investigate the elemental composition, Table 3 shows that the principal elements present in the material are silicon, calcium and aluminum—this is expected considering that PCBs usually contain these elements as it contains calcium aluminosilicate. The activation process has not disrupted the composition due to the increased thermal stability of aluminosilicate materials. However, after activation, the bromine (in the fire retardant) can be removed and recovered (by ion exchange) due to its reaction with KOH forming KBr, which is washed out during the washing process and can be collected using ion exchange (Ning et al. 2017a). This indicates that potassium

has been fixed onto the surface of the material, creating potential functional –O–K +, ion-exchange active groups (Table 3).

FTIR Analysis

Fourier transform infrared spectroscopy (FTIR) analyses were conducted to understand the changes in functionalities of the raw and activated materials. Figure 1 shows a comparison between the raw and A-NMF; it is observed that there is a substantial difference in the surface chemistry in terms of functional groups.

The spectrum of an activated NMF shows a strong and broad signal between 3250 to 3550 cm^{-1}, caused due to the stretching mode of the Si–O–X (X = K or H) functional groups. It is inferred that the dominant activation mechanism that took place on the adsorbent's surface is the breakage of the siloxane groups to form the silonol groups mainly due to the absence of hydroxyl groups before the activation process. Furthermore, due to the cage's opening, more siloxane groups appeared on the surface of the activated NMF; confirmed by the peak observed at 1013 cm^{-1}. A similar observation based on silinol groups was made in a study that conducted FTIR analysis on clay adsorbents before and after modification (Dobe et al. 2022). The surface analysis also confirms this that pores are developed during the process. The band location at 2928 cm^{-1} in the NMF spectrum shows C–H bond stretch (de Souza et al. 2022) which could be an indication of the presence of certain aliphatic groups (Hashemian et al. 2014). Additionally, C-H$_2$ groups isolated from Si were confirmed due to the vibrations at 1461 cm^{-1}. Most importantly, there is a reduction in intensities for both vibrations as the carbon is burnt off.

N$_2$ adsorption−desorption studies/ BET analysis

In order to characterize the adsorbent material, SA studies have been carried out. Table 4 shows the BET SA and the pore volume (PV) of both raw and activated material by the nitrogen gas adsorption–desorption technique.

As observed in Table 4, the raw material (NMF) is a non-porous substance possessing a very low SA of 1 m^2/g. On the other hand, the activated adsorption material (A-NMF) was shown to be mesoporous with about 222 m^2/g SA. This clearly shows the development of significant mesoporous structures due to activation. As seen in the table, the raw material, NMF, is non-porous with a SA below 1 m^2/g. In comparison, the A-NMF has a larger SA with mesopores, this demonstrates that the activation process has successfully developed a mesoporous structure.

XPS analysis

XPS examines the surface chemistry of both NMF and A-NMF. Figure 2 shows that the most prominent photoelectron peaks are present at 102, 152, 285, 293, 347 and 531 eV which represents to Si (2p), Si (2 s), C (1 s), K (2p), Ca (2p), and O (1 s), respectively. Evident from the results presented in both Fig. 2 and Table S1, an increase in intensities for O, Si, Ca, and K peaks was observed after activation; additionally, a small carbon peak is noticed on the surface of the raw the

Table 4 BET SA and PV of NMF and A-NMF

Sample	S_{BET} (m^2/g)	V_{micro} (cc/g)	V_{meso} (cc/g)	V_{total} (cc/g)	p/p_0
NMF	0.9	0.006	0	0.006	0.98
A-NMF	222	0.004	0.738	0.742	0.98

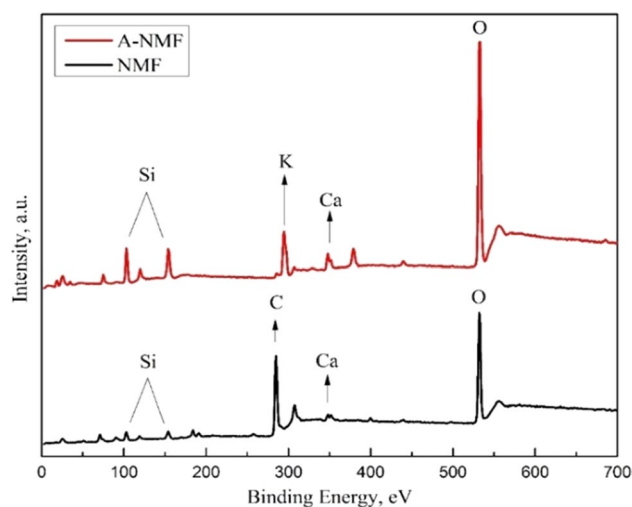**Fig. 1** FTIR Spectra of NMF and A-NMF

Fig. 2 XPS spectrum of NMF and A-NMF

activated material. This further confirms the reduction, which occurs in the carbon content after the activation process. Furthermore, the increased intensity of surface oxygen confirms oxygen atoms surfaces from the silicate network during their reaction as Si–O–K or Si–O–Ca groups. As for the raw material, oxygen atoms are exposed as reacted silanol or unreacted siloxane groups because of the siloxane functional groups' cleavage. The increase in calcium, silicon, and potassium elements also have the same justification.

SEM–EDX analysis

Figure 3 shows the SEM images of NMF (a) and A-NMF (b). The images clearly show the NMF is composed of random glass fibers with carbonaceous materials on the surface compared to amorphous A-NMF with potassium. The thermo-alkaline reaction is confirmed from the images that changed the non-porous NMF to porous clusters of A-NMF. The SEM EDX elementary mapping shows the amorphous properties of the activated material and how there is a uniform distribution of potassium on the surface of the material among other metals including calcium, silicon and calcium.
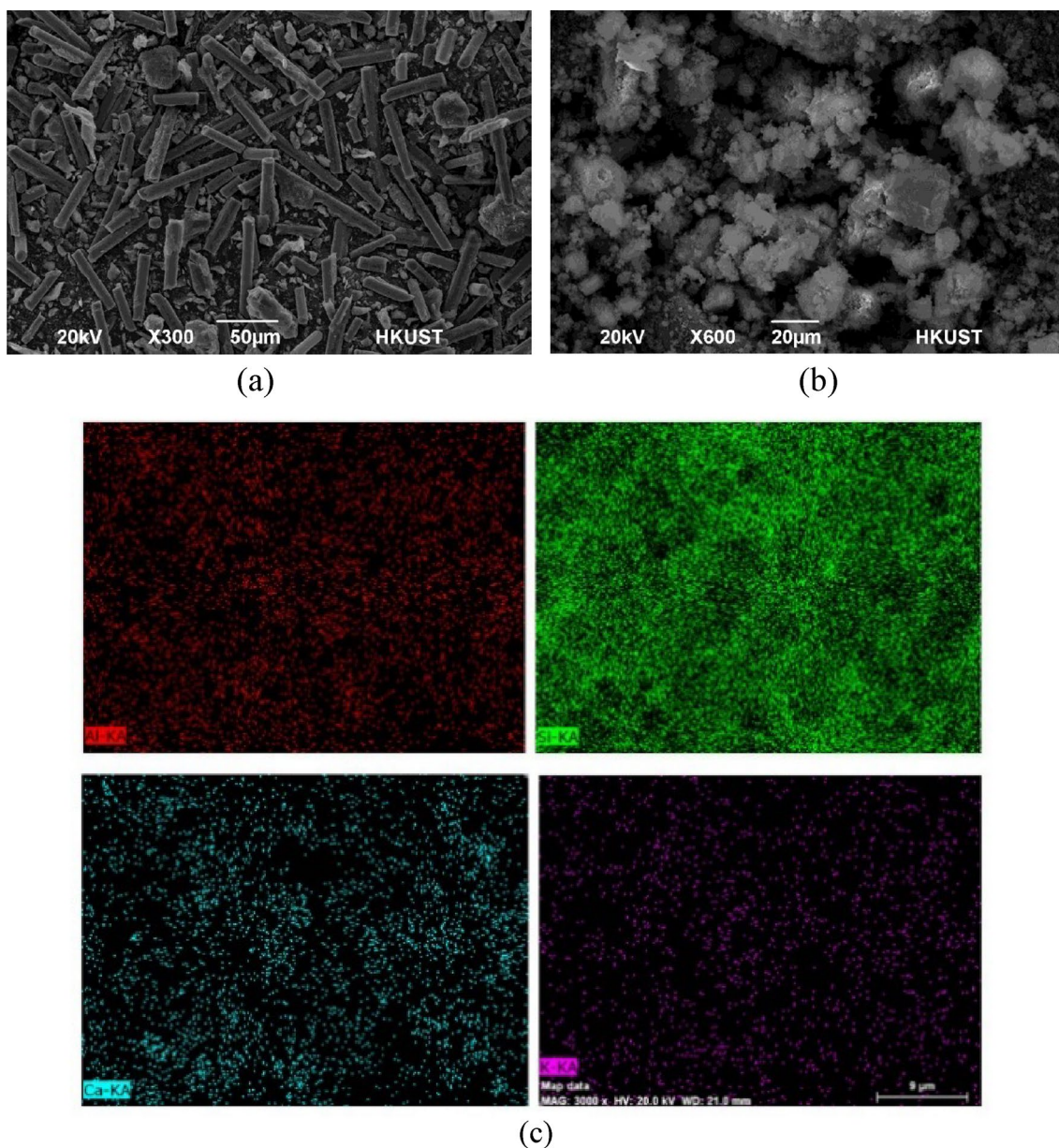
Fig. 3 a SEM image of NMF b SEM image of A-NMF c SEM–EDX elementary mapping of A-NMF

Experimental equilibrium results

It was observed that the maximum adsorption capacity for zinc metal at 2.01 mmol/g between concentrations 0–5 mmol/L (Fig. 4). The maximum adsorption capacity of zinc removal in this study is comparable with other recent studies that have been carried out (Table 5). These studies include both adsorbents derived from waste and synthetic materials, therefore, proving the effectiveness and applicability of this adsorbentthe coming sections including the regeneration and optimization of the adsorbent will further prove this point.
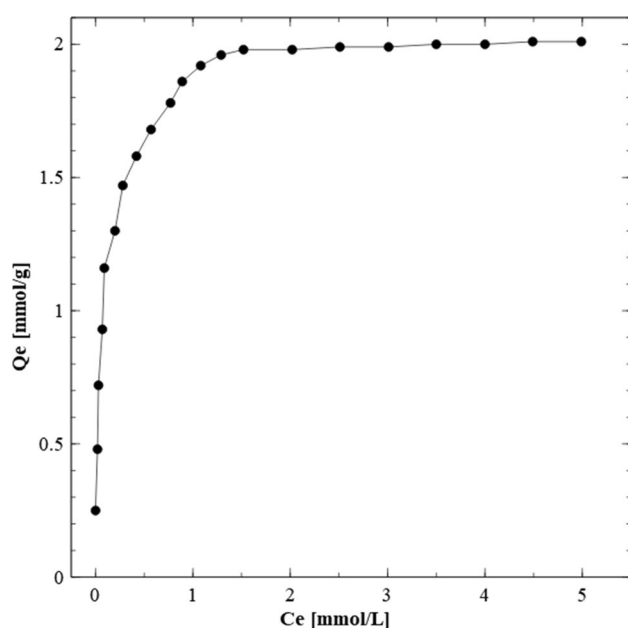
Fig. 4 Removal Efficiency of zinc (Adsorption Capacity Qe Vs final concentration Ce)

Mass balance analysis

An interesting connection between the divalent zinc adsorption capacities (Qe) and the desorption capacities (Qd) of the divalent calcium and monovalent potassium in Table S2 shows that the Qd values of Ca + 0.5 K and the Qe values of zinc are directly related and, in most cases, equal; as expected, the % error between these two values is minimal ($\leq 3.00\%$). This explains the ion exchange system that takes place in the system; technically, for every exchange/removal of a mol of zinc then it is shown that a mol of calcium is required (both metals are divalent) and 0.5 mol of potassium is exchanged (as potassium is monovalent) as shown in Fig. 5. The exchange mechanism is shown in Fig. 7. Based on the data in Table S2, we can propose that the material balance can be represented by Eq. (4):

$$Qe - Zn = Qd - Ca + 0.5Qd - K \tag{4}$$

Figure 5 is the plot of Eq. 4 showing the Zn mass balance.

Figure 5 is the plot of Eq. 4 showing the Zn removed mass balance (in black) and the amount of Ca and K exchanged into the solution Qd-Ca + 0.5 K (in green). The two curves are almost superimposed on each other justifying our proposed mechanism in Eq. 4 and suggesting that these two are the only removal mechanisms.

Isotherm models analysis

Usually, adsorption isotherms show the specific relationship between the concentration of sorbate and the degree of adsorption onto the surface at constant temperature (Zuhara et al. 2023). In this study, the experimental data at equilibrium time are correlated by the 7 isotherm models, including Langmuir, Freundlich, RP, SIPS/LF, Temkin, Toth, and DR. The Microsoft Solver program was implemented and showed that the SIPS/LF model had the best fit with the

Table 5 Zinc adsorption comparison studies

| Source of adsorbent	Type of adsorbent	Zinc adsorption capacity (mmol/g)	Study
Plant	Wood-based granular activated carbon	0.058	(Loganathan et al. 2018)
Seaweed	Alginate extraction byproduct	0.78	(Cardoso et al. 2020)
Plant	Hardwood leaf	0.098	(Shen et al. 2015)
Plant	Date stones	0.14	(Bouhamed et al. 2016)
Plant	Water Hyacinth root	0.48	(Lin et al. 2020)
Synthetic	Resin	3.00	(Bezzina et al. 2020)
Synthetic	Polyamidoamine dendrimers-decorated silica	0.42	(Wu et al. 2020)
Synthetic	Magnetic chlorapatite nanoparticles	1.18	(Keochaiyom et al. 2017)
Electronic equipment	E-waste derived adsorbent	2.01	This study
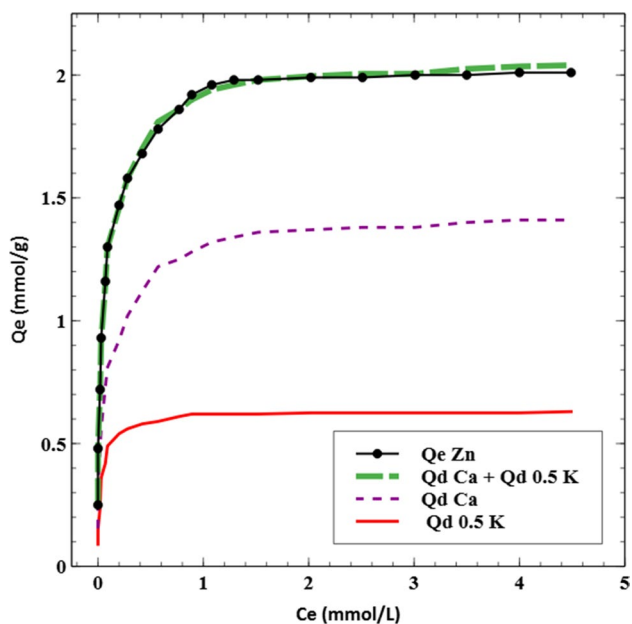
Fig. 5 Mass Balance Analysis

experimental data given that the model produced the lowest SSE (Table S3). This model is a combination of both Langmuir and Freundlich isotherm models, based on the Freundlich equation assumes that the amount of adsorbed substance increases with an increase in concentration and eventually reaches a finite limit at a particularly high concentration.

The Sips isotherm was considered the best fit in many recent adsorption studies (Andelescu et al. 2018). There are only slight variations in the maximum adsorption capacities among the models, except for the Temkin model results (Table S3). Generally, the Temkin model is considered an outstanding model in the gas phase equilibrium (where identical orientation is not required). In liquid-phase adsorption such as this study, this model's result is usually considered inappropriate (Foo and Hameed 2010). Several other recent adsorption studies on heavy metal removal found the SIPS model to be the best fit (Fil et al. 2018; Lam et al. 2019; Alkurdi et al. 2021).

Binary exchange model and analysis using desorption models

Table S4 and Figures S1 and S2 display the desorption modeling of calcium and potassium. The desorption curve seems to fit most with SIPS/ LF for calcium based on SSE error values (Table S4). As for potassium, models Langmuir, Redlich–Peterson, SIPS/LF, and Toth models showed promising results with SSE values as low as 0.04. In general, the adsorption and desorption curves showed that they follow the same kind of behavior. The maximum desorption capacities for calcium and potassium were at the maximum concentration levels; this means that at the maximum adsorption concentration of zinc, calcium, and potassium is desorbed the most and are possibly present in the solution (Fig. 6).
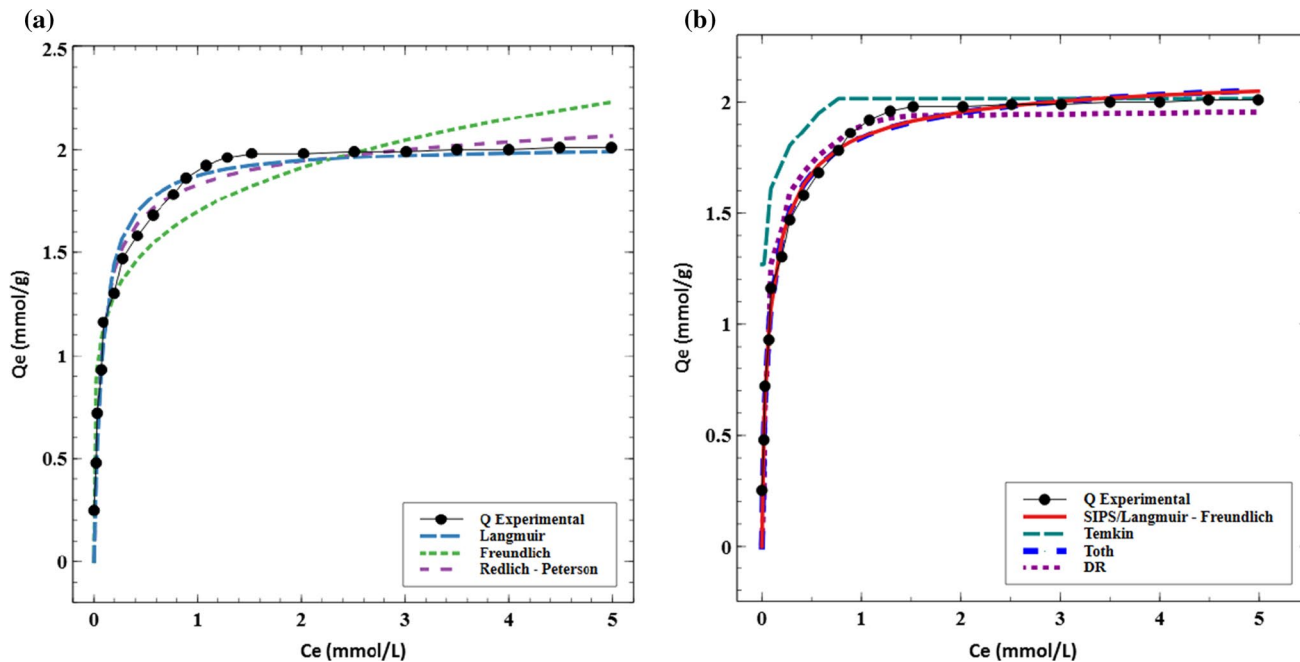
Fig. 6 Zinc Adsorption Isotherm modelling **a**- Langmuir, Freundlich, Redlich–Peterson–Peterson **b**-SIPS, Temkin, Toth, DR

Fig. 7 Schematic representation of the proposed adsorption mechanism
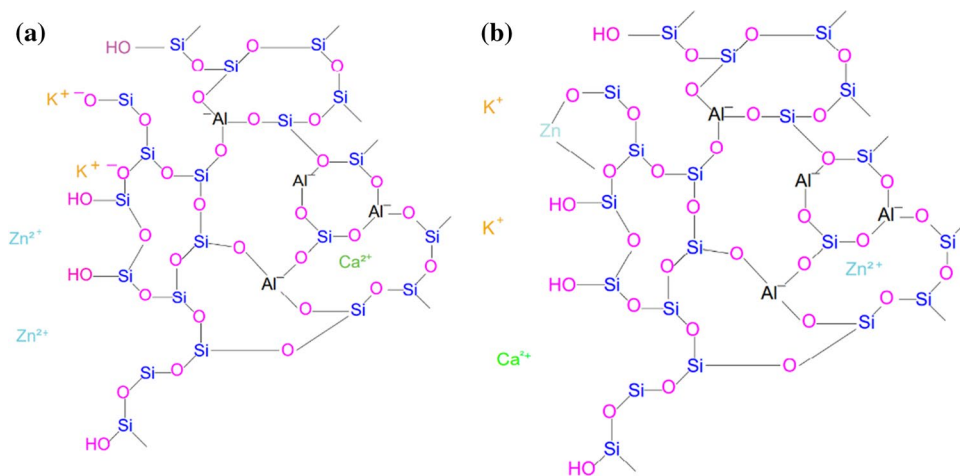
Therefore, this shows a direct correlation between the zinc adsorption model and calcium and potassium desorption models compliant with results both experimentally and theoretically. Figure 7 shows a schematic representation of the proposed mechanism of ion exchange in this study. Figure 7a reveals how the adsorbent was embedded with potassium and calcium after activation; the figure also shows the adsorbent after treatment and it is evident that the zinc ions replaced the calcium and potassium ions. This application to contaminated water systems can reduce the environmental and health impact associated with zinc. Future research should involve a study to create the successful removal and recovery of the metal from the adsorbent and its reuse for beneficial purposes.

Comparison of models

Model comparisons developed and applied in this study is presented in this section and compared with the experimental data values. The first two model results have been presented in Sects. "Mass balance analysis" and "Isotherm models analysis", namely, the mass balance Eq. (4) and the overall best first isotherm values. Since excellent fits have been obtained by SIPS model for the zinc removal and the desorption balances for calcium and potassium, the quantity of zinc adsorption can also be represented in terms of the isotherm-desorption equations by inputting SIPS model equation (Table 1) for calcium and potassium in Eq. 5. This incorporation results in a novel model Eq. (6) that can be used for such a binary system. The numerical values of the constants in Eq. (6) are inputted in Eq. (7).

$$Qe - Zn = Qd - Ca + 0.5Qd - K \tag{5}$$

$$Qe - Zn = \frac{K_{LF,Ca}Ce^{nLF-Ca}}{1 + a_{LF-Ca}Ce^{nLF-Ca}} + \frac{0.5[KLF, KCe^{nLF-K}]}{[1 + a_{LF-K}Ce^{nLF-K}]} \tag{6}$$
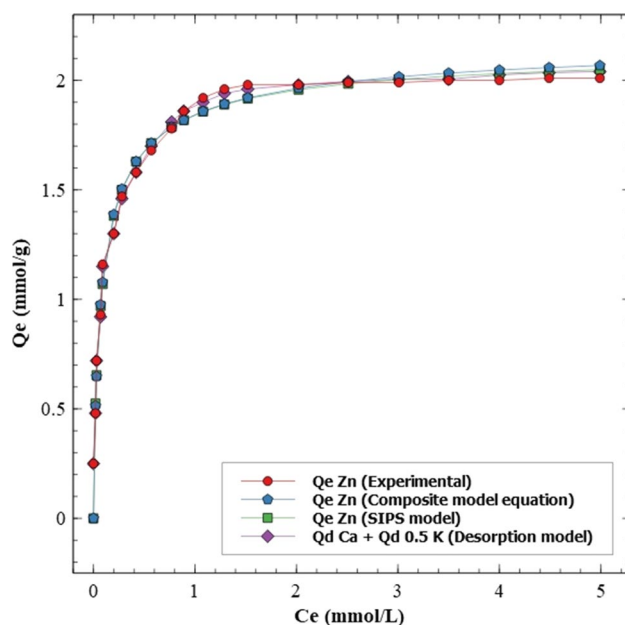
Fig. 8 Comparing experimental, composite model equation, SIPS, desorption model adsorption capacities

$$Qe - Zn = \frac{5.76Ce^{0.66}}{1 + 3.66\,Ce^{0.66}} + \frac{13.35\,Ce^{1.03}}{1 + 21.0\,Ce^{1.03}} \tag{7}$$

This is the simplified composite model equation that can be used to calculate the adsorption capacity of zinc in a binary system involving calcium and potassium. Table S5 shows the adsorption capacities of zinc from different calculations in this study including experimental, desorption model, calculated SIPS model and the proposed composite equation model. The composite Eq. (4) aligns perfectly with the other models (Table S5) with zero mean square error (MSE) when compared to the adsorption capacities of the other models. This shows the validity of the models and how the composite equation can be used to give accurate results

Table 6 Comparison of zinc removal capacity before and after regeneration

Cycle number	Metal	Loading capacity (mmol/g)	Fraction Zn recovered in acid	Final adsorption capacity (mmol/g)	Change in adsorption capacity from previous stage
1	Zinc	2.05	0.92	1.65	
2		1.65	0.88	1.25	Decreased by 32%
3		1.25	0.82	0.84	Decrease by $\approx$ 49%

in such a system; Fig. 8 shows a visual representation of how the three models behave similarly in accordance with the experimental values.

Regeneration and reuse

Only preliminary regeneration experiments were performed in the present study to re-use the adsorbent. Nitric acid was tested as the regenerating medium and three concentrations, 0.1, 0.2 and 0.3 M, were used for two contact times, 5 and 10 min. The results for the two contact times showed no difference. However, the different acid concentrations were quite significant. At 0.1 M nitric acid 85% of the adsorbed zinc was removed, at 0.2 M nitric acid 92% adsorbed zinc was removed, however, at 0.3 M acid concentration the aluminosilicate resin began to dissolve, so no further studies were carried out above 0.2 M nitric acid concentration.

The regeneration results for three regenerations are presented in Table 6 for 0.2 M nitric acid for five minutes contact time. Post recovery of zinc, and backwashing using water for many times before filtering and drying. Two to three rounds of zinc removal were conducted. The results are presented in Table 6, showing that the removal capacity decreased by 32% in the second stage and a further reduction of 49% was observed in the final stage.

A reason for the additional decrease in adsorption capacity at each reuse cycle, as shown in the last column in Table 6, is the increased hydrogen ions in the functional adsorption sites after the regeneration process- this makes it difficult for the zinc to exchange with the calcium and potassium ions.

Optimization for minimizing adsorbent mass

Figure 9 shows a two-stage equilibrium stage adsorption system. L_s is the volume of polluted water treated in each stage using different mass (M) of adsorbent in stage 1 and stage 2. The concentrations of solutions are expectedly reduced from the initial influent (C_o) the first (C_1) and second stages (C_2); alternatively, the initial pollutant concentration on the adsorbent, first stage, and second stage (labeled q_0, q_1, q_2, respectively), increases as the stages go with initial concentration being zero.

The material balance equations for the two stages are given below:

For stage 1:

$$L_s(C_0 - C_1) = M_1(q_1 - q_0) \tag{8}$$

For stage 2:

Fig. 9 Schematic representation of adsorbent mass optimization
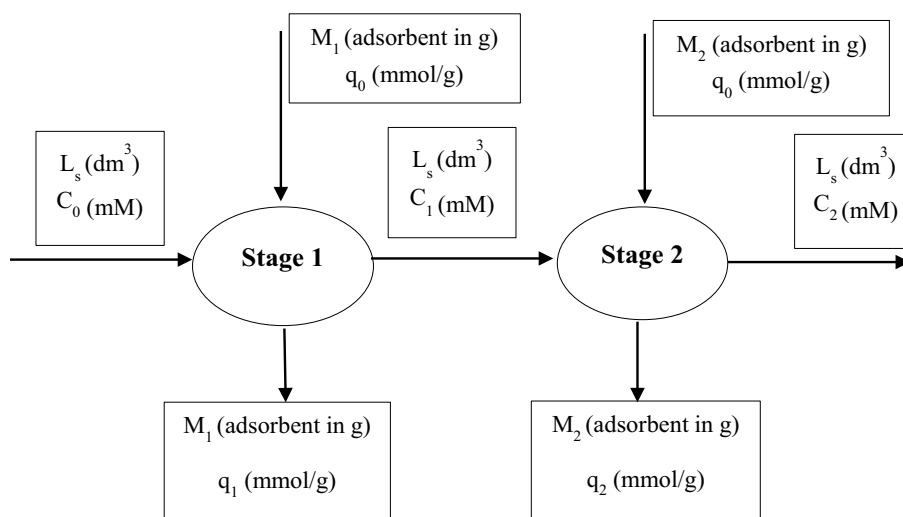
$$L_s\left(C_1 - C_2\right) = M_2\left(q_2 - q_1\right) \qquad (9)$$

The SIPS equation used for isotherm modelling previously will be used for further derivation:

$$q_e = \frac{K_{LF} C_e^{n_{LF}}}{1 + a_{LF} C_e^{n_{LF}}}$$

The material balance for stage 1 after substituting the SIPS equation for q_1 when $q_0 = 0$ becomes:

$$\frac{M_1}{L_s} = \frac{\left(C_0 - C_1\right)\left(1 + a_{LF} C_1^{nLF}\right)}{K_{LF} C_1^{nLF}} \qquad (10)$$

Similarly for the second stage:

$$\frac{M_2}{L_s} = \frac{\left(C_1 - C_2\right)\left(1 + a_{LF} C_2^{nLF}\right)}{K_{LF} C_2^{nLF}} \qquad (11)$$

To check the total amount of adsorbent used, the two equations, namely, 10, and 11, are added and simplified to make $\frac{d\left[(M_1 + M_2)/L_S\right]}{dC_1} = 0$ (to minimize adsorbent amount), and the final equation obtained is:

$$X = \left(\frac{C_1}{C_2}\right)^{b_F} - b_F \frac{C_0}{C_1} - 1 + b_F \qquad (12)$$

The mass required is calculated after determining C_1 (this will vary with different pollutant removal rates) by keeping $X = 0$ while keeping the initial concentration values according to the experimental data for all cases. According to the isotherm model results, the SIPS model fit best to the adsorption data obtained using this adsorbent. Therefore, this design will utilize this model for the calculations (see above); the designing was carried out for fixed pollutant removal rates of 99%, 95%, 90%, 85%, 80% to understand how much adsorbent mass will be required for each of these cases.

Table S6 shows the estimated mass required for zinc removal at 99% removal efficiency (both two-stage and single-stage adsorption systems). The optimization for the two-staged system reveals that for the two-stage system, the mass of adsorbent required in the first stage is much higher than the second stage as the uptake is fast when the adsorption process begins. After adding the adsorbent from both stages, it is evident that the amount required for all cases is less than the minimum amount of adsorbent required using a single stages system. For example, the design for 99% of the two-stage adsorption system requires only ≤0.324 g for zinc removal compared to ≤0.336 g using a single-stage batch adsorber. The difference is more significant at lower initial concentrations- for example, an initial concentration of 0.25 mmol/L only requires 0.026 g for a two-stage adsorption system, contrary to the single-stage system that requires 0.176 g. However, this proves that two small reactors can save the amount of adsorbent needed, especially for low-capacity adsorbents.
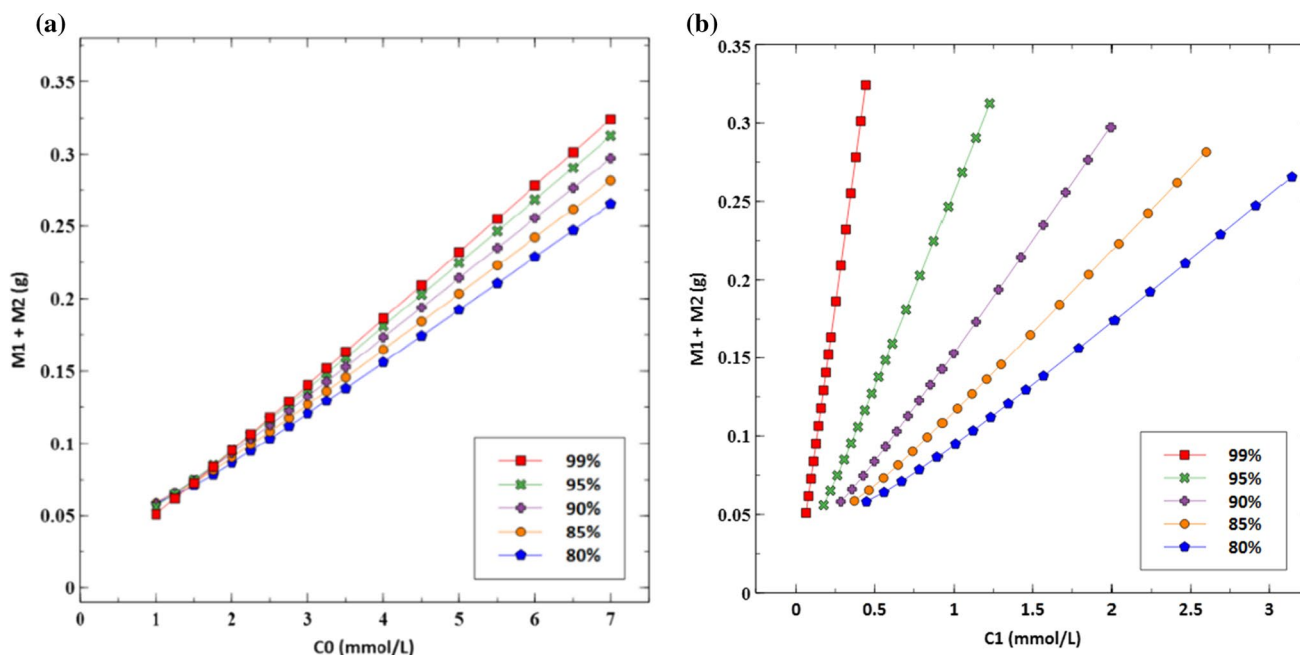

Fig. 10 Total adsorbent mass required for a two-stage reactor for different removal efficiencies against **a** initial pollutant concentration **b** intermediate pollutant concentration

The results in Table S6 show how the total mass of adsorbent required increases when the removal efficiency rises. Figure 10 shows the trend of total mass of adsorbent used in all the five cases; this makes it clear that the total mass required in only slightly higher when the removal efficiency is higher, and this difference is more when the initial concentration is higher.

Conclusion

This study shows high removal capacities for zinc using the alkali modified aluminosilicate ion exchange material from PCB e-waste by following a binary ion exchange system with calcium and potassium. The maximum adsorption capacity of zinc reaches a maximum of 2.01 mmol/g between concentrations 0 and 5 mmol/L. The high adsorption capacity shows how well this adsorbent works; it is observed to be comparable and, in most cases, better than the adsorption capacities using synthetic and waste adsorbents (Table 5). The isotherm analysis of zinc's adsorption data shows that the SIPS model is the best fit as it had the lowest SSE value.

A novel model based on the mechanism between zinc adsorption and calcium and potassium desorption is developed based on the mass balance analysis. The quantitative desorption studies on calcium and potassium further confirm this unique interaction that enables the effective removal of zinc to be predicted. The novel composite equation derived shows excellent similarity with the mass balance and isotherm modelled adsorption capacities and can therefore be used in the future for a binary system. In conclusion, this adsorbent derived from waste is attractive for zinc removal from water and the novel model enables an accurate adsorption treatment system to be designed for future purposes. Based on the SSE error after isotherm modelling on the zinc adsorption data reveals SIPS model as the best fit model. Further optimization calculations based on SIPS model using a two-stage reactor system demonstrated a lower adsorbent requirement making the system more economical. Future experiments on upscaling the proposed reactor system and associated techno-economic studies are necessary.

Declarations

References

Alkurdi SSA, Al-Juboori RA, Bundschuh J et al (2021) Inorganic arsenic species removal from water using bone char: a detailed study on adsorption kinetic and isotherm models using error functions analysis. J Hazard Mater 405:124112. https://doi.org/10.1016/j.jhazmat.2020.124112

Andelescu A, Nistor MA, Muntean SG, Rădulescu-Grad ME (2018) Adsorption studies on copper, cadmium, and zinc ion removal from aqueous solution using magnetite/carbon nanocomposites. Sep Sci Technol 53:2352–2364. https://doi.org/10.1080/01496395.2018.1457696

Bezzina JP, Robshaw T, Dawson R, Ogden MD (2020) Single metal isotherm study of the ion exchange removal of Cu(II), Fe(II),

Pb(II) and Zn(II) from synthetic acetic acid leachate. Chem Eng J 394:124862. https://doi.org/10.1016/j.cej.2020.124862

Bilal M, Ihsanullah I, Younas M, Ul Hassan Shah M (2022) Recent advances in applications of low-cost adsorbents for the removal of heavy metals from water: a critical review. Sep Purif Technol 278:119510. https://doi.org/10.1016/j.seppur.2021.119510

Bouhamed F, Elouear Z, Bouzid J, Ouddane B (2016) Multi-component adsorption of copper, nickel and zinc from aqueous solutions onto activated carbon prepared from date stones. Environ Sci Pollut Res 23:15801–15806. https://doi.org/10.1007/s11356-015-4400-3

Cardoso SL, Costa CSD, Da Silva MGC, Vieira MGA (2020) Insight into zinc(II) biosorption on alginate extraction residue. Kinetics, isotherm and thermodynamics. J Environ Chem Eng 8:103629. https://doi.org/10.1016/j.jece.2019.103629

Carolin CF, Kumar PS, Saravanan A et al (2017) Efficient techniques for the removal of toxic heavy metals from aquatic environment—a review. J Environ Chem Eng 5:2782–2799. https://doi.org/10.1016/j.jece.2017.05.029

Çelebi H, Gök G, Gök O (2020) Adsorption capability of brewed tea waste in waters containing toxic lead(II), cadmium (II), nickel (II), and zinc(II) heavy metal ions. Sci Rep 10:1–12. https://doi.org/10.1038/s41598-020-74553-4

Chakraborty R, Asthana A, Singh AK et al (2022) Adsorption of heavy metal ions by various low-cost adsorbent—a review. Int J Environ Anal Chem 102:342–379. https://doi.org/10.1080/03067319.2020.1722811

Cherono F, Mburu N, Kakoi B (2021) Adsorption of lead, copper and zinc in a multi-metal aqueous solution by waste rubber tires for the design of single batch adsorber. Heliyon 7:e08254. https://doi.org/10.1016/j.heliyon.2021.e08254

de Souza CC, de Souza LZM, Yılmaz M et al (2022) Activated carbon of Coriandrum sativum for adsorption of methylene blue: Equilibrium and kinetic modeling. Clean Mater 3:100052. https://doi.org/10.1016/j.clema.2022.100052

Dobe N, Abia D, Tcheka C et al (2022) Removal of amaranth dye by modified Ngassa clay: linear and non-linear equilibrium, kinetics and statistical study. Chem Phys Lett 801:139707. https://doi.org/10.1016/j.cplett.2022.139707

Dubinin MM (1960) Surface and nanomolecular catalysis. Zhur Phys Chem 34:959

Fil BA, Yilmaz AE, Boncukcuoğlu R, Bayar S (2018) Kinetics and isotherm analysis of Cd^{2+} removal from aqueous solutions by ion exchange process. Environ Eng Manag J 17:1967–1976. https://doi.org/10.30638/EEMJ.2018.196

Foo KY, Hameed BH (2010) Insights into the modeling of adsorption isotherm systems. Chem Eng J 156:2–10. https://doi.org/10.1016/j.cej.2009.09.013

Freundlich H (1926) Colloid and capillary chemistry. Methuen, London, pp 6–8

Hadi P, Ning C, Ouyang W et al (2015) Toward environmentally-benign utilization of nonmetallic fraction of waste printed circuit boards as modifier and precursor. Waste Manag 35:236–246. https://doi.org/10.1016/j.wasman.2014.09.020

Hashemian S, Salari K, Yazdi ZA (2014) Preparation of activated carbon from agricultural wastes (almond shell and orange peel) for adsorption of 2-pic from aqueous solution. J Ind Eng Chem 20:1892–1900. https://doi.org/10.1016/j.jiec.2013.09.009

Joseph L, Jun BM, Flora JRV et al (2019) Removal of heavy metals from water sources in the developing world using low-cost materials—a review. Chemosphere 229:142–159. https://doi.org/10.1016/j.chemosphere.2019.04.198

Keochaiyom B, Wan J, Zeng G et al (2017) Synthesis and application of magnetic chlorapatite nanoparticles for zinc (II), cadmium (II) and lead (II) removal from water solutions. J Colloid Interface Sci 505:824–835. https://doi.org/10.1016/j.jcis.2017.06.056

Lam YY, Lau SSS, Wong JWC (2019) Removal of Cd(II) from aqueous solutions using plant-derived biochar: kinetics, isotherm and characterization. Bioresour Technol Rep 8:100323. https://doi.org/10.1016/j.biteb.2019.100323

Langmuir I (1918) A new adsorption isotherm. Langmuir I(40):1361–1403

Lestari AYD, Chafidz A, Hapsari AR et al (2020) Magnetically modified corn cob as a new low-cost biosorbent for removal of Cu (II) and Zn (II) from wastewater. J Bahan Alam Terbarukan 9:96–102. https://doi.org/10.15294/jbat.v9i02.27136

Lin S, Huang W, Yang H et al (2020) Recycling application of waste long-root Eichhornia crassipes in the heavy metal removal using oxidized biochar derived as adsorbents. Bioresour Technol 314:123749. https://doi.org/10.1016/j.biortech.2020.123749

Loganathan P, Shim WG, Sounthararajah DP et al (2018) Modelling equilibrium adsorption of single, binary, and ternary combinations of Cu, Pb, and Zn onto granular activated carbon. Environ Sci Pollut Res 25:16664–16675. https://doi.org/10.1007/s11356-018-1793-9

Mangwandi C, Suhaimi SNA, Liu JT et al (2016) Design, production and characterisation of granular adsorbent material for arsenic removal from contaminated wastewater. Chem Eng Res Des 110:70–81. https://doi.org/10.1016/j.cherd.2016.04.004

Mariyam S, Cochrane L, Zuhara S, McKay G (2022a) Waste management in qatar: a systematic literature review and recommendations for system strengthening. Sustain 14:1–23. https://doi.org/10.3390/su14158991

Mariyam S, Zuhara S, Al-Ansari T et al (2022b) Novel high capacity model for copper binary ion exchange on e-waste derived adsorbent resin. Adsorption 28:185–196. https://doi.org/10.1007/s10450-022-00360-0

Mendret J, Azais A, Favier T, Brosillon S (2019) Urban wastewater reuse using a coupling between nanofiltration and ozonation: techno-economic assessment. Chem Eng Res Des 145:19–28. https://doi.org/10.1016/j.cherd.2019.02.034

MuthuramanUthara PS, Akash R, Korkai A (2020) Preparation and Characterisation of activated carbon from e-waste and its application on dye decolourization. J Ind Pollut Control 36:2258–2265

Ning C, Hadi P, Xu M et al (2016) Valorization of an electronic waste-derived aluminosilicate: surface functionalization and porous structure tuning. ACS Sustain Chem Eng 4:2980–2989. https://doi.org/10.1021/acssuschemeng.5b01523

Ning C, Hadi P, Aghdam E et al (2017a) Environmental emission analysis of a waste printed circuit board-derived adsorbent production process. Chem Eng J 326:594–602. https://doi.org/10.1016/j.cej.2017.05.181

Ning C, Lin CSK, Hui DCW, McKay G (2017b) Waste printed circuit board (PCB) recycling techniques. Top Curr Chem 375:21–56. https://doi.org/10.1007/s41061-017-0118-7

Nowicki P, Kazmierczak-Razna J, Skibiszewska P et al (2016) Production of activated carbons from biodegradable waste materials as an alternative way of their utilisation. Adsorption 22:489–502. https://doi.org/10.1007/s10450-015-9719-z

Parthasarathy P, Zuhara S, Al-Ansari T, McKay G (2023) A review on catalytic CO_2 pyrolysis of organic wastes to high-value products. Fuel 335:127073. https://doi.org/10.1016/j.fuel.2022.127073

Rahman KO, Aziz KHH (2022) Utilizing scrap printed circuit boards to fabricate efficient Fenton-like catalysts for the removal of pharmaceutical diclofenac and ibuprofen from water. J Environ Chem Eng 10:109015. https://doi.org/10.1016/j.jece.2022.109015

Redlich OJDL, Peterson DL (1959) A useful adsorption isotherm. J Phys Chem 63:1024–1024

Shen Z, Jin F, Wang F et al (2015) Sorption of lead by Salisbury biochar produced from British broadleaf hardwood. Bioresour Technol 193:553–556. https://doi.org/10.1016/j.biortech.2015.06.111

Shrestha R, Ban S, Devkota S et al (2021) Technological trends in heavy metals removal from industrial wastewater—a review. J Environ Chem Eng 9:105688. https://doi.org/10.1016/j.jece.2021.105688

Sips R (1948) On the structure of a catalyst surface. J Chem Phys 16:490–495

Temkin MI (1940) Kinetics of heterogeneous catalysis. J Phys Chem 14:1153–1158

Terdputtakun A, Arqueropanyo OA, Sooksamiti P et al (2017) Adsorption isotherm models and error analysis for single and binary adsorption of Cd(II) and Zn(II) using leonardite as adsorbent. Environ Earth Sci 76:1–11. https://doi.org/10.1007/s12665-017-7110-y

Toth J (1971) Groundwater discharge: a common generator of diverse geologic and morphologic phenomena. Int Assoc Sci Hydrol Bull 16:7–24. https://doi.org/10.1080/02626667109493029

Turkmen Koc SN, Kipcak AS, Moroydor Derun E, Tugrul N (2021) Removal of zinc from wastewater using orange, pineapple and pomegranate peels. Int J Environ Sci Technol 18:2781–2792. https://doi.org/10.1007/s13762-020-03025-z

Van Hien N, Valsami-Jones E, Vinh NC et al (2020) Effectiveness of different biochar in aqueous zinc removal: correlation with physicochemical characteristics. Bioresour Technol Rep 11:100466. https://doi.org/10.1016/j.biteb.2020.100466

Wu K, Luan L, Xing JX et al (2020) Removal of Zn(II) and Co(II) from N, N-dimethylformamide by polyamidoamine dendrimers decorated silica: performance and mechanism. J Mol Liq 308:113073. https://doi.org/10.1016/j.molliq.2020.113073

Wu C, Awasthi AK, Qin W et al (2022) Recycling value materials from waste PCBs focus on electronic components: technologies, obstruction and prospects. J Environ Chem Eng 10:108516. https://doi.org/10.1016/j.jece.2022.108516

Xu M, Alyasi H, Ning C et al (2021) Removal of toxic cadmium using a binary site ion-exchange material derived from waste printed circuit boards. J Chem Technol Biotechnol 96:3282–3292. https://doi.org/10.1002/jctb.6866

Zhang D, Sial MS, Ahmad N et al (2021) Water scarcity and sustainability in an emerging economy: a management perspective for future. Sustain 13:1–10. https://doi.org/10.3390/su13010144

Zuhara S, Pradhan S, Mckay G (2023) Investigating mixed biosolids and cardboard for methylene blue adsorption: activation, adsorption modelling and thermodynamics. Environ Res 225:115534. https://doi.org/10.1016/j.envres.2023.115534